SPE 164062-MS

Laboratory Studies for Surfactant Flood in Low-Temperature, Low-Salinity Fractured Carbonate Reservoir

Aparna Raju Sagi, Maura Puerto, Yu Bian, Clarence A. Miller, and George J. Hirasaki, Rice University, Mehdi Salehi, and Charles P. Thomas, TIORCO, Jonathan T. Kwan, Kinder Morgan.

This paper was prepared for presentation at the SPE International Symposium on Oilfield Chemistry held in The Woodlands, Texas, USA, 8–10 April 2013.

Abstract

The objective was to identify surfactants for Enhanced Oil Recovery by brine-oil interfacial tension reduction for a carbonate reservoir at ~ 25ºC and salinity of ~11,000ppm TDS; thus, Alkyl Propoxy Sulfates and their blends with sulfonates were evaluated to determine optimal salinity and solubilization parameters with dead crude. Imbibition experiments were performed in reservoir and dolomite outcrop cores to determine the oil recovery efficiency of surfactant systems, selected from their phase behavior test results, with potential to recover oil. Tridecyl alcohol 13 propoxy sulfate (TDS-13A) with an oil solubilization parameter of ~8 at reservoir salinity was found to recover greater than 75% oil in imbibition experiments, at a concentration as low as 0.5wt%. The adsorption of surfactants on dolomite was measured at static and dynamic conditions; the adosprtion of TDS-13A was found to be ~ 0.26 – 0.34 mg/g reservoir rock. The effect of solution gas on surfactant phase behavior, up to 600-psi, was evaluated for methane, ethane, carbon-dioxide, and separator gas at 30ºC. Methane had minimal effect on surfacatant optimal salinity, lowering it by ~2%/100psi solution gas, followed by carbon-dioxide which reduced it by ~11%/100psi. Ethane had a much more pronounced effect, reducing optimal salinity by ~46%/100psi solution gas.

Introduction

Enhanced Oil Recovery (EOR) in carbonate reservoirs with the use of surfactants has previously been demonstrated in both laboratory (Standnes et al., 2003; Hirasaki et al., 2004; Lu et al. 2012) and field studies (Chen et al., 2001; Rilian et al., 2010). Fractured oil-wet carbonate reservoirs tend to have a high percentage of original oil in place (OOIP) after forced displacement because, the injected fluids flow predominantly in the high permeability fractures, while most of the oil remains trapped in the low permeability matrix by capillary forces. Surfactants can reduce the brine-oil interfacial tension (IFT) to ultra-low values ($<10^{-3}$ mN/m) and/or alter the wettability of the rock to being preferentially water-wet, thereby overcoming the capillary forces that trap the oil. To achieve this, a surfactant or surfactant blend has to be tailored to the reservoir conditions: temperature, salinity (total dissolved solids (TDS), total hardness (TH)), crude oil. This paper describes laboratory studies that were performed to select a surfactant formulation, for a constant salinity EOR process in a fractured carbonate reservoir, at low temperature (~ 25°C) and low salinity (~ 11,000 ppm TDS; ~1,700ppm TH) conditions, and to determine the effect of solution gas on surfactant phase behavior at 30°C.

Some of the desirable characteristics of a surfactant flood in a fractured carbonate reservoir are: ultra-low brine-oil IFT, wettability alteration from oil-wet to water wet condition, clear solutions in injection and reservoir brine, tolerance to divalent ions, thermal stability, no generation of viscous phases or emulsions, low surfactant rentenion by adsorption and phase trapping, mobility control for improved distribution of injected fluids in the fracture network, and easy separation of oil from produced emulsion. Wettability alteration, mobility control and emulsion separation were not addressed in this study. Anionic, cationic and nonionic surrfactants have all been used for IFT reduction. In this study we evaluated Alkyl Propoxy (PO) Sulfates (APS) and their blends with Internal Olefin Sulfonates (IOS), an Alkyl Benzene Sulfonate (ABS) and an Alkyl Xylene Sulfonate (AXS).

For a given set of conditions (temperature, oil type, etc), surfactants may achieve ultra-low IFTs only in a range of salinitiy near optimal salinity. APSs and their blends with IOSs reported in other studies (Aoudia et al., 1995; Levitt et al., 2009; Barnes et al., 2010) have shown high solubilization parameter, an indicator of IFT reduction, but at optimal salinities or temperatures higher than those of this study. The PO groups of APSs lend tolerance to divalent ions, and provide a way to increase lipophilicity of the surfactant by adding more POs. IOSs by themselves have poor divalent ion tolerance (Liu et al.,

2008) and the availability of IOSs with long hydrocarbon chains is limited. A surfactant blend might have an increased solubility limit compared to either surfactant by itself (Liu et al., 2008). Also, branching of the surfactant hydrocarbon chains, and the presence of PO groups, helps to avoid the formation of viscous phases and eliminate the use of alcohol (Hirasaki et al., 2011), which has the disadvantage of reducing solubilization parameter (Salter, 1977) and in turn increasing the minimum IFT achievable.

Due to ease of handling, dead oil is used instead of live oil in most studies of surfactant systems evaluated with crude oil. A few studies have been performed to study the effect of pressure and solution gas, mainly methane, on surfactant phase behavior. The effect of pressure alone tends to increase the optimal salinity (Skauge et al., 1990; Austad et al., 1996, Roshanfekr et al., 2012), while increasing amount of methane as solution gas seems to decrease the optimal salinity (Nelson, 1983; Puerto et al., 1983, Roshanfekr et al., 2012; Southwick et al., 2012). In this study, we show the effect solution gas on optimal salinity, for methane, ethane and carbon dioxide up to 600psi, the pressure in the reservoir of interest.

Experimental Procedure

Materials.

Surfactants.

Surfactants are listed in Table 1. Surfactant concentration is expressed in wt%, as the weight (in gm) of active surfactant per 100ml of aqueous phase.

Brines.

The composition of reservoir brine, Brine 1 (Br1), is given in Table 2, but when prepared in the laboratory, a precipitate was formed. In order to avoid precipitation, the bicarbonate was replaced with equal moles of chloride, Brine 2 (Br2). Most experiments were with Br2. When Br1 was to be used, two separate stable brines were prepared, one with all the divalent ions, and another with all the bicarbonate, and these brines were then mixed in-situ in the presence of surfactant when required.

Oil.

The dead crude oil was centrifuged for 40 minutes at 5000 rpm. A small amount of brown colored phase, suspected to be emulsified oil, separated from the oil. The dead crude oil had a density of 28.2 ºAPI and viscosity of 22.5cP at 25°C. IFT of the dead crude oil measured against DI water was 25 mN/m, and against 2 %NaCl was 18 mN/m. Total Acid Number of the crude oil is 0.80 ± 0.01 mg KOH/g oil.

Phase behavior.

Dead oil.

Aqueous phase (surfactant, brine, DI water) and oil were added in a water oil ratio (WOR) of ~1, to a sealed bottom 2ml or 5ml glass pipette, and the open end was then sealed using an oxyacetylene flame torch. The samples were mixed at the test tempeature in a rotating mixer for ~24 hrs, and were then allowed to stand to let the phases separate under the action of gravity.

Live oil.

Live oil phase behavior samples were made in a high-pressure sight cell tested for 1000psi. For the samples with pure gas, the cell was purged with the gas before a known volume of dead crude (~4ml±0.5ml) was added to the cell at 25ºC. When synthetic separator gas was used, the headspace, above the loaded dead crude oil, was purged by pressurizing it to 600psi and releasing the pressure.The test gas was then introduced into the headspace at the test pressure, and the cell was rocked to allow the gas to dissolve in the oil. This was repeated till the oil was assumed saturated with the gas because the test pressure remained constant after mixing. The change in the oil volume was noted. Known volume of surfactant solution (~4ml±0.5ml) was then introduced slowly into the cell, while bleeding off the excess pressure. The cell was placed at 30°C for a day, to allow the contents of the cell to reach the test temperature. The cell was then rocked by hand to allow the contents to mix. If the pressure fell short or exceeded the test pressure (in almost all cases, the difference was not more than 10% of the desired pressure), more gas was added or excess gas was purged. The sample was mixed by hand multiple times over several days, till the resulting equilibriated phases did not change in volume and appearance. A schematic of the procedure is shown in Figure 1. Separator gas composition listed in Table 3 was based on reservoir fluid analysis data. All gases were obtained from Matheson.

Optimal salinity and solubilization parameter.

The classical Winsor surfactant phase behavior transitions from Type I to Type III to Type II microemulsions with increasing salinity. The optimal salinity falls in the Type III region, and is the salinity at which solubilization parameters σ_o, σ_w of oil and water in the microemulsion phase are equal, as this corresponds to a minimum in the IFT (Haely et al., 1976). However, in almost all the phase behavior scans with crude oil reported in this study, Type III microemulsions were not observed. Based on the change in level of the oil/water (o/w) interface after equilibriation, the solubilization parameters σ_o and σ_w were calculated as V_o/V_s and V_w/V_s, assuming that all the surfactant was in the microemulsion phase. Optimal salinity was determined based on the following criteria:

1. In salinity scans of ~0.1Br2 or 0.2%NaCl salinity intervals, optimal salinity was selected as the salinity of the last Type I sample before inversion to Type II. For salinity intervals coarser than 0.1Br2 or 0.2%NaCl, optimal salinity was selected at mid-point of the interval at which transition from Type I to Type II was observed.

2. If V_o/V_s in Type I region continues to decrease with increasing salinity before reaching a clear inversion to Type II, then the optimal salinity is taken as that where the maximum value of V_o/V_s was measured. For salinities beyond this maximum, lipophilic species of this commercial surfactant may partition into the oil and/or emulsion may form. Because the presence of viscous emulsions is undesirable, one might choose not to inject surfactant solutions above the optimal salinity as chosen here.

A high solublizatoin parameter (>10) corresponds to ultra-low IFT. Solubilization parameter was used as an indicator of IFT reduction, and no IFT measurements were made for any of the surfactant systems discussed in this paper.

Viscosity of phases.

The viscosity of the equilibriated phases for the surfactant-brine-dead oil phase behavior samples was measured using a falling sphere viscometer developed by Lopez-Salinas et al. (2009). A gold-coated stainless steel sphere, 0.774mm in diameter, was introduced into the 5ml pipette in which the phase behavior sample was being prepared. Figure 2 shows a schematic of the set-up. The sphere was dropped from the top of the sample, and four sensors recorded the time at which the sphere passed through them. Based on the transit time of the sphere through each section between a pair of sensors, the average viscosity of the phase(s) in that section was computed. The height of each section was ~4.5cm.

Imbibition.

Imbibition experiments were conducted in both dolomite outcrop and reservoir cores. The reservoir cores were cleaned by Dean-Stark extraction. The cores were saturated with brine under vacuum, followed by flooding with crude oil to initial water saturation. After being aged at 90ºC for a month, the cores were placed in an imbibition cell filled with brine for at least 20 days and then the brine was replaced with clear surfactant solution. The oil recovery reported is the excess oil recovered, and it does not account for oil solubilized in Type I microemulsions formed in the cell during the experiment.

Adsorption.

Static adsorption.

Known amounts of dolomite powder or crushed reservoir rock, and surfactant solutions of different concentrations were encased in vials and mixed by rotation for ~24 hours. The samples and blanks (no dolomite added) were centrifuged at 5000rpm for 30 minutes. Surfactant concentrations were determined by potentiometric titration against TEGO. BET surface area of the dolomite powder, crushed reservoir rock, and the reservoir rock (cut into 2mm – 5mm size pieces) was measured.

Dynamic adsorption.

Dynamic adsorption measurements were performed in reservoir dolomite cores and a limestone sandpack. The sandpack was prepared by dry sieving limestone sand, washing the 20-40 mesh fraction with water to remove the fines, and drying it in the oven before packing it compactly into a glass column. The 1.5-inch reservoir dolomite cores cleaned with toluene, tetrahydrofuran and chloroform, were placed in a rubber sleeve in a coreholder, and an overburden pressure of ~ 1000psi was applied with water. Air was vacuumed out of the core under a vacuum of ~28-29 inHg. Pore volume was measured by saturating the core/sandpack with brine under vacuum. Surfactant solution containing non-adsorbing bromide tracer (bromide replaced an equimolar amount of chloride) was passed through the core/sandpack at a fixed rate for several pore volumes. Bromide concentration was measured using a bromide electrode and the surfactant concentration was measured by Epton two-phase titration against Hyamine with methylene blue indicator. The pressure drop across the core/sandpack was monitored by a pressure transducer.

Results and discussion

Phase behavior.

Dead oil at 25ºC.

Table 4 summarizes optimal salinity of the various surfactants and their blends evaluated at 25°C with dead crude oil. NI blend (S1/S2 80:20) (Liu, 2008) showed good divalent ion tolerance and IFT reduction with a West Texas crude oil similar to the one used in this study. However, as the optimal salinity of the blend, ~5%NaCl + 1% Na_2CO_3, was much higher than the reservoir salinity, a more lipophilic IOS, S3 was blended with S1. The optimal salinity as a function of blend ratio for this blend decreases with increasing fraction of S3, to ~3% NaCl for S1/S3 10:90 blend, which is still higher than reservoir salinity. As increasing the hydrophobe size would lower the optimal salinity, TDS-13B and TDS-13A, which are the same surfactants but made from different feedstocks, were evaluated. A salinity scan of 2wt% TDS-13B shows that a Type I microemulsion exists up to 1.0Br2, but the oil/microemulsion interface drops after 0.8Br2 as shown in Figure 3. In accordance with the previous criteria, optimal salinity is taken as 0.8 Br2. For 2wt% TDS-13A 1.0Br2 and 1.25 Br2 were found to be Type I, and 1.5Br2 was found to be Type II. Because the transition from Type I to Type II occurred close to reservoir salinity, salinity scans with a finer salinity interval were performed at different surfactant concentrations of 0.25wt%, 0.5wt% and 4wt% (Figure 4), to determine optimal salinity precisely, and to see the effect of dilution on optimal salinity. The optimal salinity was 1.4Br2 at 4wt% surfactant concentration and was reduced to 1.2Br2 and 1.3Br2 at 0.5wt% and 0.25wt%. Thus, with dilution, TDS-13A remains in the Type I region at 1.0 Br2 (reservoir salinity), but close to optimal salinity. This behavior is in contrast with 1wt% TDS-13A/A6/C8 blend (TAC blend) + 0.25wt% EGBE co-solvent, which becomes Type II with dilution. Such surfactant phase behavior becoming Type II with dilution is undesirable as this would cause retardation of the surfactant front in the reservoir due to phase trapping, and the generation of viscous macroemulsions as was observed in the Type II

regime for many of the surfactant systems analyzed in this study. Based on the 4wt% salinity scan, TDS-13A has σ_o of ~8 at reservoir salinity of 1.0Br2.

Viscosity of phases.

Figure 5 shows photograph of the salinity scan of 0.5wt% TDS-13A with crude oil after settling for 16 days. The transition from Type I to Type II occured between 1.15Br2 and 1.26Br2 (same as in Figure 4). Figure 5 shows the viscosities of the upper phase (oil/Type II microemulsion), lower phase (brine/Type I microemulsion), and middle section (upper phase + lower phase + macroemulsion phases if present). The upper phase viscosity remained close to that of crude oil for all of the samples measured. The viscosity of oil/water microemulsion was between 2cP and 3cP for salinities between 0.84Br2 and 1.15Br2. For 1.36Br2 and 1.47Br2, the lower phase looked like clear brine, and the viscosity was expected to be close to that of brine, but the measured value was higher. This could be because emulsion (from the middle section) was observed to be sticking to the sphere as it dropped through the brine phase. Of importance is the average viscosity of the middle section, which drastically increased with salinity when reaching the Type II region. The high average viscosities (100-300cP) for 1.36Br2 and 1.47Br2 were caused by the macroemulsion present at the oil/water interface of those samples, and the actual viscosities of these phases would be much higher than the average when the thicknesses of these phases are taken into account. Generation of these viscous macroemulsions in the Type II region was observed in other systems as well. This makes it undesirable to operate in this region when designing a chemical flood.

Imbibition.

Four 3-inch long Silurian outcrop dolomite core plugs (D1 – D4) cut from a single foot long core, had similar permeabilities 195±15mD, porosities 14-16%, and initial oil saturation ~0.70. These were used to test for oil recovery by imbibition using 0.5wt% TDS-13A and 1wt% TDS-13A/A6/C8 blend +0.25wt EGBE, both of which had optimal salinity of ~1.2Br2 at 25°C, and compare their oil recovery efficiencies with NI blend and N91-8, both of which are known to be away from optimal conditions at reservoir salinity. As can be seen in Figure 6, both TDS-13A and TAC blend performed well, recovering ~75% of the oil, while the NI blend and N91-8 recovered only about 47% and 25% of the oil respectively.

Figure 7 compares the imbibition profiles for 1wt% TAC blend + 0.25wt% EGBE, in reservoir core (R1) and outcrop core (D1). The imbibition recovery history and final recovery are very similar in both cases, though the permeability and initial oil saturation are quite different. In Figure 8, the effect of TDS-13A surfactant concentration on the oil recovery in reservoir cores (R2, R3) is shown. The final oil recovery at 0.25wt% TDS-13A was substantially lower than that at 0.5wt%, probably because IFT was higher at the lower surfactant concentration. Final oil recovery in both reservoir and outcrop cores are the same for 0.5wt% TDS-13A. Table 5 summarizes all the imbibition experiments.

Adsorption.

Static adsorption.

Static adsorption experiments were carried out at 25°C, on dolomite powder (1.18 m^2/g surface area) for TDS-13A and TAC blend (Figure 9). The adsorption isotherms are Langmuir type. The absence or presence of bicarbonate in brine did not seem to have an effect on the plateau adsorption, but the presence of alcohol seems to increase the adsorption. The plateau adsorption for TAC blend with 0.25wt% EGBE is the same ~5.2 mg/m^2 for both brines, Br1 and Br2; Br1 has ~2900ppm bi-carbonate that is replaced with equivalent moles of chloride in Br2. TDS-13A by itself has plateau adsorption of ~ 2.3mg/m^2, while addition of 0.25wt% EGBE to TDS-13A, increases the adsorption to ~ 3.7 mg/m^2. For the same brine and EGBE content, TDS-13A/A6/C8 blend has a higher adsorption than TDS-13A.

Dynamic adsorption.

Three dynamic adsorption experiments were performed to estimate the adsorption of TDS-13A at 25°C. The adsorption data was fit to the analytical solution Eq. 1 of a one-dimensional flow, linear adsorption isotherm model for dynamic adsorption.

$$C = 0.5 erf(\eta) \quad (1)$$

where,

$$\eta = \frac{1 - \frac{t_D}{1+\beta}}{2\sqrt{\frac{t_D}{Pe(1+\beta)}}}$$

$$Pe = \frac{Lv}{K_l};\ \beta = \frac{C_s}{C_l} = \frac{(1-\phi)}{\phi}\rho S k_{ads};\ t_D = \textit{pore volume throughput}$$

β, obtained by the best fit of this model to the experimental data, can be used to compute the cord-slope of the adsorption isotherm k_{ads}, and the adsorption for the given concentration. β=0 is used to fit the model for the bromide tracer data.

Figure 10 - Figure 12. show the normalized effluent concentration plotted as a function of the pore volumes produced, and Table 6 summarizes the experimental parameters and calculated adsorption for all the three experiments. The adsorption on limestone sand was computed by fitting the experimental data of Figure 10 to be 0.29 mg/g sand, or 0.13 mg/g reservoir rock after correcting for surface areas of the sand (~0.36 m^2/g) and reservoir rock (~0.16 m^2/g). This is much lower than the static adsorption value of TDS-13A ~ 0.34mg/g rock, possibly because the flow rate was too fast for reaching equilibrium adsorption. The residence time was ~6hr, which is one fourth the equilibriation time for the static adsorption experiment. The same reason explains the drop in effluent surfactant concentration at ~1.7PV in the dynamic adsorption in a 6mD reservoir core (Figure 11) when the experiment was shut in for a day. Two model fits can be made for the data before and after the shut-in, giving two values of adsorption, ~0.06 mg/g rock and ~0.26 mg/g rock, the latter being much closer to the static adsorption value. Figure 12 shows the effluent concentrations for dynamic adsorption in a 15mD reservoir core, carried out with a residence time of about ~30hr to allow adsorption to reach equilibrium. The computed value of adsorption is ~0..26mg/g rock, similar to the previous experiment after shut-in. Note however that for the experiments in reservoir cores the effluent surfactant concentration reached a plateau at ~0.8 normalized concentration, and did not reach injection concentration. Also, the pressure drop across the core, at a constant flow rate, increased with increasing pore volumes injected into the core, for both cores. The pressure history for the 15mD core is shown in Figure 12. The injection solution for this experiment first passed through a 2µm filter, and the pressure drop across the filter remained fairly constant over the time of the experiment. This pressure behavior, and the plateauing of surfactant concentration at 80% injected concentration, is an indication of surfactant either precipitating in the core or getting filtered out there.

Effect of solution gas on surfactant phase behavior at 30ºC.

The optimal salinity of TDS-13A decreased with increase in temperature from 25ºC to 30 ºC, so it was blended with a more hydrophilic surfactant S2 to increase the optimal salinity to close to 1.0Br2. 1wt% TDS-13A/S2 90:10 which had an optimal salinity of ~0.9Br2 with dead crude oil (Figure 13) was tested for the effect of solution gas on surfactant-crude oil phase behavior. The surfactant blend was evaluated with methane, ethane, carbon dioxide, and separator gas. Figure 14 - Figure 20 show photographs of samples from surfactant salinity scans for these gases at different pressures and the phase maps of the equilibrated systems. Two pressure cells with different dead volumes and slightly different cross sectional areas were used for the live oil experiments. These two factors combined with the variation in the total volume of the phases (~8ml±1ml) are responsible for the different heights of the samples seen in the photographs.

Figure 14, at 600psi methane, shows that for 0.9Br2 and 1.1Br2, a macroemulsion and excess brine were in "equilibrium" with a phase which seems to be mostly oil, making these Type II microemulsions, while 0.5Br2 and 0.7Br2 exhibited Type I microemulsions. The optimal salinity for this system was determined to be ~0.8±0.1Br2, the average of the salinity range over which the transition from Type I to Type II occurred, as the salinity increment was coarse.

Figure 15 and Figure 16 show surfactant salinity scans of ethane at 50psi and 95psi. At 50-psi, 0.5Br2 – 0.7Br2 were Type I microemulsions, while 0.8Br2 was a Type II microemulsion. The oil solubilization parameter σ_o at 0.7Br2 was ~13, and this was chosen to be the optimum due to the high σ_o. This was the only sample where the change in the level of the oil/microemulsion interface after equilibration was substantial enough to make a determination of solubilization parameter. At 95psi ethane, 0.3Br2 - 0.5Br2 were Type I microemulsions, while 0.6Br2 was a Type II with a macroemulsion and excess brine phase. 0.6Br2 could be misinterpreted as a Type III microemulsion, but after careful observation, it was concluded to be a macroemulsion instead. The optimal salinity for this system was determined to be ~0.5Br2.

Figure 17 and Figure 18 show surfactant salinity scans at 60psi and 600psi carbon dioxide. At 60psi CO_2, 0.7Br2 and 0.8 Br2 were Type I microemulsions, while 1.0Br2 is a Type II microemulsion. 0.9Br2 looked like a Type I microemulsion based on the color of the aqueous phase, but could be interpreted as a Type II because the oil/water interface seemed to have moved lower than the initial o/w interface. Due to this ambiguity, the optimal salinity was determined to be 0.85Br2±0.05Br2. At 600psi carbon-dioxide, 0.2Br2 and 0.3Br2 are Type I while 0.5Br2 is a Type II microemulsion, with a large macroemulsion phase. Similar to 0.9Br2 at 60psi carbon-dioxide, classification of 0.4Br2 at 600psi as Type I or Type II was ambiguous; while the aqueous phase seemed colored making it a Type I, the intensity of light transmitted through the aqueous phase at 0.4Br2 when observed in a dark room with a light source from behind the sight cell, made the aqueous phase look like it had much less oil solubilized (similar to the aqueous phases observed at 1.3Br2 and 1.4Br2 in the salinity scan of 0.5wt% TDS-13A in Figure 3). Due to this ambiguity, the optimal salinity was interpreted to be ~0.35Br2±0.05Br2.

In Figure 19, optimal salinity as a function of solution-gas pressure is plotted for the three pure gases. While methane appeared not to decrease optimal salinity much with increase in pressure (~1.8%/100psi), carbon dioxide (~10%/100psi) and ethane (~46%/100psi) caused a much greater drop in optimal salinity.

Figure 20 shows the salinity scan at 600psi separator gas from 0.2Br2 – 0.5Br2. The sample at 0.3Br2 was prepared by diluting the sample at 0.35Br2 with 1wt% surfactant in DI water. The 0.5Br2 sample was Type II in "equilibrium" with macroemulsion, while 0.2Br2 – 0.35Br2 samples appeared to be Type I; in spite of the increasing salinity, the intensity of color of the lower phase microemulsion decreased from 0.25Br2 to 0.35Br2, which could imply decreasing amount of oil solubilized. Optimal salinity would be 0.425Br2±0.075Br2 based on the transition from Type I to Type II, or ~0.25Br2 based on decreasing intensity color in the lower phase. The drop in optimal salinity from dead to live oil is 50% - 70%. This result indicates that the amounts of carbon dioxide, ethane, and higher molecular weight hydrocarbons which dissolved in the dead crude oil were sufficient to change microemulsion phase behavior substantially, even though their concentrations in the initial

separator gas were low (Table 3). Note that (a) final composition of gas in the head space differs from that of Table 3 owing to differential solution of various species in the oil and (b) the live oil formed in this experiment is different from reconstituted live oil in that the latter is to be prepared by taking the separator gas and dead crude oil in a certain ratio (which depends on the solution gas oil ratio) and pressurizing it to 600psi to dissolve the gas in the oil. This was not done as the solution gas oil ratio for the separator gas was not available. Also note that the separator gas (in the headspace) to crude oil ratio differs from sample to sample. While this would not make a difference for the experiments with pure gases, it would result in differing oil compositions when a gas mixture is used because of the oil phase being enriched in the more soluble gas with increasing gas to oil ratio.

Conclusions

1. Optimal salinity close to reservoir salinity (~11,000ppm) at 25°C was obtained by using a surfactant with a large hydrophobe, TDS-13A (Tridecyl alcohol 13PO sulfate). Measured oil solubilization parameter for this surfactant was ~8 at reservoir salinity. Oil recovery efficiency in imbibition experiments in aged dolomite cores was >75% at 0.5wt% surfactant concentration, but dropped to ~45% at 0.25wt% surfactant concetration.
2. 1wt% TDS-13A/A6/C8 60:10:30 + 0.25wt% EGBE was also identified to have an optimal salinity close to reservoir salinity at 25ºC, and performed well in imbibition experiments, ~70% oil recovery. But the optimal salinity decreased drastically with dilution, shifting system phase behavior to Winsor Type II.
3. Adsorption of TDS-13A on dolomite measured by static adsorption on dolomite powder (~0.34mg/g rock) and dynamic adsorption in reservoir cores (~0.26mg/g rock) are comparable at 25°C. However, for the dynamic adsorption experiments in cores, the effluent surfactant concentration reached a plateaue at ~80% injection concentration, and the pressure across the core increased with volume throughput, indicating plugging of the core.
4. Effect of solution gas on surfactant phase behavior for TDS-13A/S2 90:10 was evaluated at 30 ºC. Live oil made with separator gas at 600psi decreased optimal salinity by ~50% - 70% compared to that with dead oil. Pure methane, ethane and carbon dioxide decreased optimal salinity by ~2%, ~46%, and ~11% repectively, per 100psi of solution gas in this system.

Nomenclature

C = Normalized concentration
C_s = Surfactant concentration on solid
C_l = Surfactant concentation in liquid
L = Length
K_l = Dispersion co-efficient
k_{ads} = Chord slope of adsorption isotherm
ϕ = Porosity
ρ = Density
σ = Solubilization parameter
S = Surface area of material
t_D = Pore volume throughput
V = Volume
υ = interstitial velocity

References

Aoudia, M., Wade, W.H., and Weerasooriya, V. 1995. Optimum Microemulsions Formulated with Propoxylated Guerbet Alcohol and Propoxylated Tridecyl Alsohol Sodium Sulfates. *Journal of Dispersion Science and Technology* 16(2), 155-135.

Austad, T., and Strand, S. 1996. Chemical Flooding of Oil Reservoirs 4. Effects of Temperature and Pressure on the Middle Phase Solubilization Parameters Close to Optimum Flood Conditions. *Colloids and Surfaces, A* 108 (2-3), 243-252.

Barnes, J.R., Dirkzwager, H., Smit, J.R., Smit, J.P., On, A., Navarrete, R.C., Ellison, B.H., Buijse, M.A., and Rijswijk, B.V. 2010. Application of Internal Olefin Sulfonates and Other Surfactants to EOR. Part 1: Structure – Performance Relationships for Selection at Different Reservoir Conditions. SPE 129766 paper presented at SPE Improved Oil Recovery Symposium, Tulsa, Oklahoma, 24-28 April.

Chen, H.L., Lucas, L.R., Nogaret, L.A.D., Yang, H.D., and Kenyon, D.E. 2001. Laboratory Monitoring of Surfactant Imbibition Using Computerized Tomography. *Society of Petroleum Engineers Reservoir Evaluation and Engineering* 4(1), 16-25.

Healy, R.N., Reed, R.L., and Stenmark, D.G. 1976. Multiphase Microemulsion Systems. *Society of Petroleum Engineers Journal* 16(3), 147-160.

Hiraksai, G., and Zhang, D.L. 2004. Surface Chemistry of Oil Recovery From Fractured, Oil-Wet, Carbonate Formations. *Society of Petroleum Engineers Journal* 9(2), 151-162.

Hirasaki, G.J., Miller, C.A., and Puerto, M.C. 2011. Recent Advances in Surfactant EOR, *Society of Petroleum Engineers Journal* 16(4), 889-907.

Levitt, D.B., Jackson, A.C., Heinson, C., Britton, L.N., Malik, T., Dwarakanath, and V., Pope, G.A. 2006. Identification and Evaluation of High-Performance EOR Surfactants. *Society of Petroleum Engineers Reservoir Evaluation and Engineering* 12(2), 243-253.

Liu, S., Zhang, D.L., Yan, W., Puerto, M., Hirasaki, G.J., and Miller, C.A. 2008. Favorable Attributes of Alkaline-Surfactant-Polymer Flooding. *Society of Petroleum Engineers Journal* 13, 5-16.

Lu, J., Goudarzi, A., Chen, P., Kim, D.H., Britton, C., Delshad, M., Mohanty, K. Weerasooriya, U.P., and Pope, G.A. 2012. SPE 159979 presented at SPE Annual Technical Conference and Exhibition, San Antonio, Texas, 8-10 October.

Nelson, R.C. 1983. The Effect of Live Crude on Phase behavior and Oil-Recovery Efficiency of Surfactant Flooding Systems, *Society of Petroleum Engineers Journal* 23(3), 501-510.

Puerto, M.C. and Reed, R.L. 1983. A Three-Parameter Representation of Surfactant/Oil/Brine Interaction. *Society of Petroleum Engineers Journal* 23(4), 669-682.

Rilian, N.A., Sumestry, M., and Wahyuningsih 2010. Surfactant Stimulation to Increase Reserves in Carbonate Reservoir: "A Case Study in Semoga Field". SPE130060 paper presented at SPE EUROPEC/EAGE Annual Conference and Exhibition, Barcelona, Spain, 14-17 June.

Roshanfekr, M., Johns, R.T., Pope, G.A., Britton, L., Britton, C., and Vyssotski, A. 2012. Simulation of the Effect of Pressure and Solution Gas on Oil Recovery From Surfactant/Polymer Floods. *Society of Petroleum Engineers Journal* 17(3), 705-716.

Salter, S.J. 1977. The Influence of Type and Amount of Alcohol on Surfactant-Oil-Brine Phase Behavior and Properties. SPE 6843 presented at SPE Annual Technical Conference and Exhibition, Denver, Colorado, 9-12 October.

Salinas, J.L., Miller, C.A., Yoo, K.H.Y., Puerto, M., and Hirasaki, G.J. 2009. Viscometer for Opaque, Sealed Microemulsion Samples. SPE121575 presented at SPE International Symposium on Oilfield Chemistry, Woodlands, Texas, 20-22 April.

Skauge, A. and Fotland, P. 1990. Effect of Pressure and Temperature on the Phase Behavior of Microemulsions. *Society of Petroleum Engineers Reservoir Engineering* 5(4), 601-608.

Southwick, J.G., Svec, Y., Chilek, G., and Shahin, G.T. 2012. Effect of Live Crude on Alkaline/Surfactant Polymer Formulations: Implications for Final Formulation Design. *Society of Petroleum Engineers Journal* 17(2), 352-361.

Standnes, D.C., and Austad, T. 2003. Wettability alteration in carbonates: Interaction between cationic-surfactant and carboxylates as a key factor in wettability alteration from oil-wet to water-wet conditions", *Colloids and Surfaces A: Physiochemical Engineering Aspects* 216, 243-259.

Table 1 List of Surfactants

Surfactant name	Formula
S1	C16-17 7PO sulfate
TDS-7	C13 7PO sulfate
TDS-13B, TDS-13A	C13 13PO sulfate
S2	C16-17 internal olefin sulfonate
S3	C20-24 internal olefin sulfonate
A6	C16-18 branched alkyl xylene sulfonate
C8	C8-10 branched alkyl benzene sulfonate
N 91-8	C9-11 8EO alcohol
NI blend	S1/S2 80:20
TAC blend	TDS-13A/A6/C8 60:10:30
TDS-13A/S2 blend	TDS-13A/S2 90:10

Table 2 Composition of Brines

Ions (ppm)	Brine 1 (Br1)	Brine 2 (Br2)	Brine 3 (Br3)
Sodium	3,026	3,026	2,660
Calcium	271	271	281
Magnesium	241	241	291
Chloride	4,099	5787	6,237
Bicarbonate	2,901	0	0
Sulfate	87	87	0
Total Dissolved Solids (TDS)	10,625	9,412	9,469

Table 3 Seperator gas composition

Component	Content (%)
Methane	65.8
Carbon-dioxide	10.0
Ethane	8.9
Propane	6.3
Butane	3.9
Iso-butane	2.6
Nitrogen	2.5

Table 4 Surfactant optimal salinity with dead crude oil at 25ºC

Surfactant	Surfactant concentration (wt%)	Optimal Salinity
S1/S3 80:20	1.0	4.25% NaCl
S1/S3 50:50	2.0	3.75% NaCl
S1/S3 10:90	2.0	3% NaCl
TDS-13B	2.0	0.8 Br2
TDS-13A	0.25	1.3 Br2
TDS-13A	0.5	1.2 Br2
TDS-13A	4.0	1.4 Br2
TDS-13A/A6/C8 60:10:30 +0.25 wt% EGBE	1.0	1.4 Br1
TDS-13A/A6/C8 60:10:30 +0.188 wt% EGBE	0.75	0.9 Br1
TDS-13A/A6/C8 60:10:30 +0.125 wt% EGBE	0.5	0.6 Br1

Table 5 Summary - Imbibition experiments at 25ºC

Core	Surfactant formulation	Length (in)	Diameter (in)	Porosity (%)	Permeability (mD)	S_{oi}	Oil Recovery (%)
D1	TAC blend 1wt% +0.25wt% EGBE	3.0	1.5	16.2	210	0.68	~76
D2	NI blend 1wt%	3.0	1.5	13.7	181	0.70	~48
D3	TDS-13A 0.5wt%	2.7	1.5	15.4	184	0.69	~75
D4	N91-8 1wt%	2.9	1.5	14.3	206	0.69	~26
R1	TAC blend 1wt% +0.25wt% EGBE	3.0	1.5	13.1	81	0.55	~68
R2	TDS-13A 0.25wt%	1.1	1.0	13.0	151	0.55	~47
R3	TDS-13A 0.5wt%	1.2	1.0	14.2	126	0.83	~80

Table 6 Summary – dynamic adsorption experiments at 25ºC

Parameters	Sandpack	Core 1	Core 2
Diameter (cm)	3.8	3.8	3.8
Length (cm)	28.0	10.0	14.9
Pore volume (ml)	72	12	30
Porosity (%)	22.5	10.5	17.7
Permeability (mD)	1.02×10^{5}	6	15
Injection solution	0.5wt% TDS-13A + 1000ppm Br^-	0.5wt% TDS-13A + 1000ppm Br^-	0.5wt% TDS-13A + 1000ppm Br^-
Flow rate (ml/h)	12	2	1
Residence time (hr)	6	6	30
Surface area (m^2/g)	0.36	0.16	0.16
β	0.19±0.005	0.31±0.03; 1.3±0.05	0.7±0.1
Adsorption (mg/g reservoir rock)	0.127±0.003	0.063±0.006 0.263±0.010	0.260±0.037

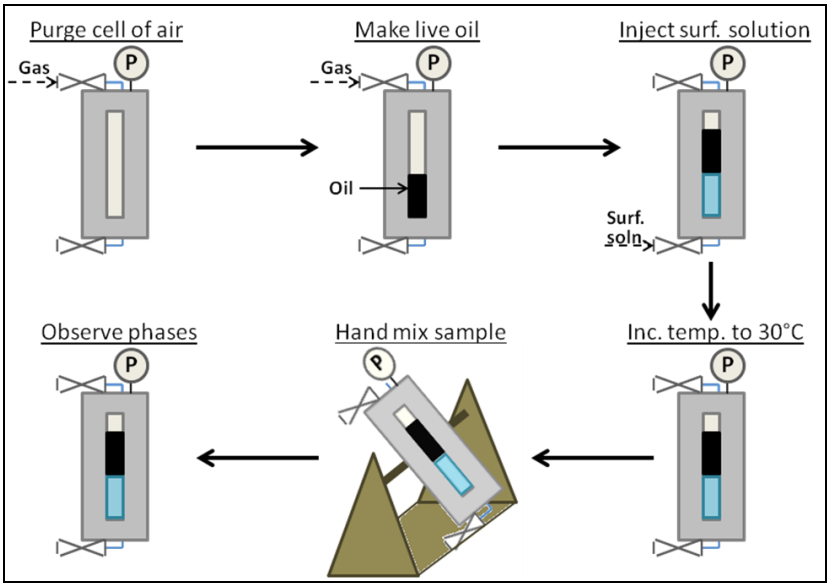

Figure 1 Experimental procedure for live oil-surfactant-brine phase behavior

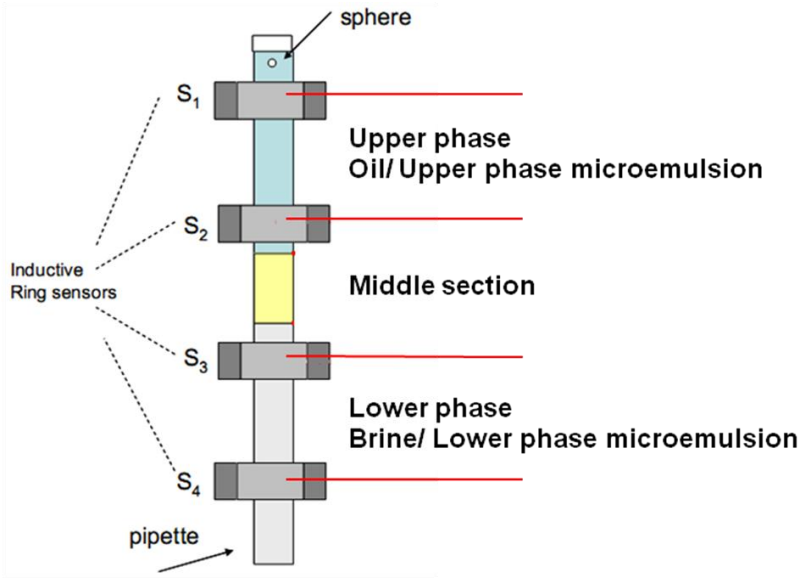

Figure 2 Experimental procedure for measurement of viscosity of phases in surfactant-brine-oil phase behavior samples. (modified from Salinas et al., 2009)

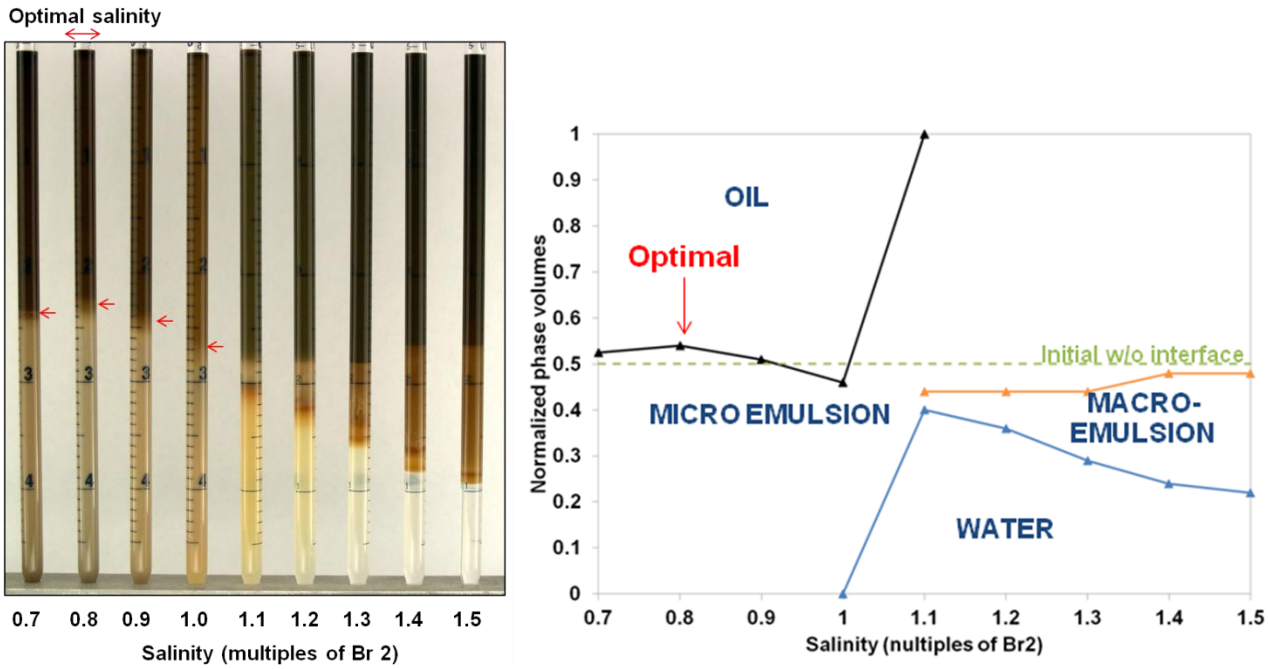

Figure 3 Salinity scan of TDS-13B 2wt% with dead crude oil at 25ºC.Arrows in the picture show the microemulsion/oil interface, which drops in the Type I region before the phase behavior transitions to Type II : non-classical phase behavior

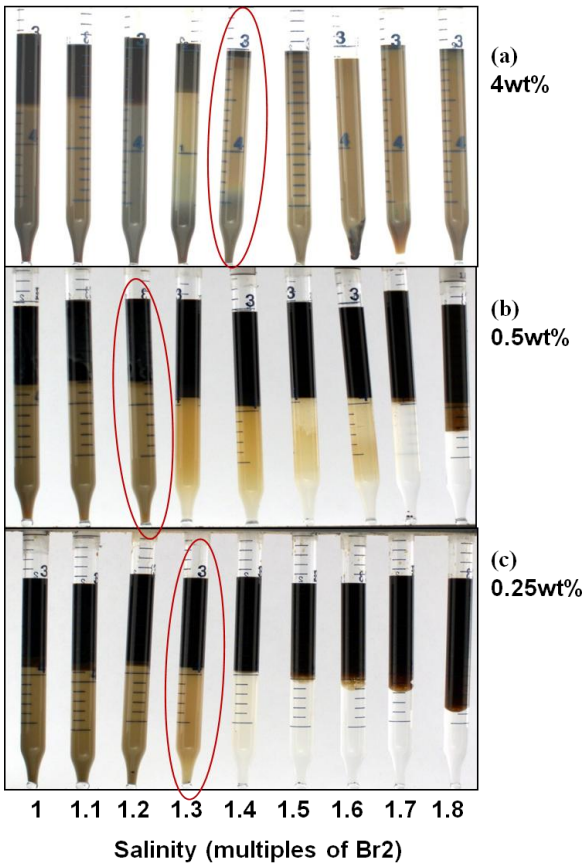

Figure 4 Salinity scan of TDS-13A at different concentrations, with dead crude oil crude oil at 25°C. Optimal salinity for each scan is encircled.

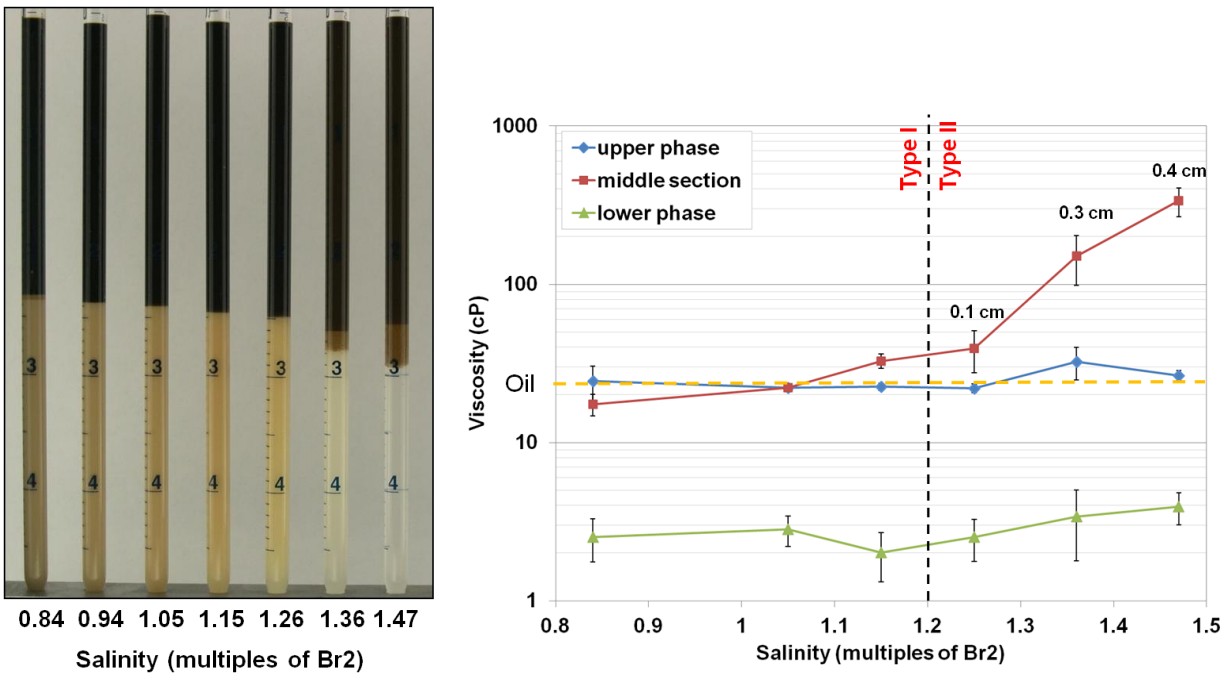

Figure 5 Viscosity of phases: TDS-13A 0.5wt% with dead crude oil at 25°C

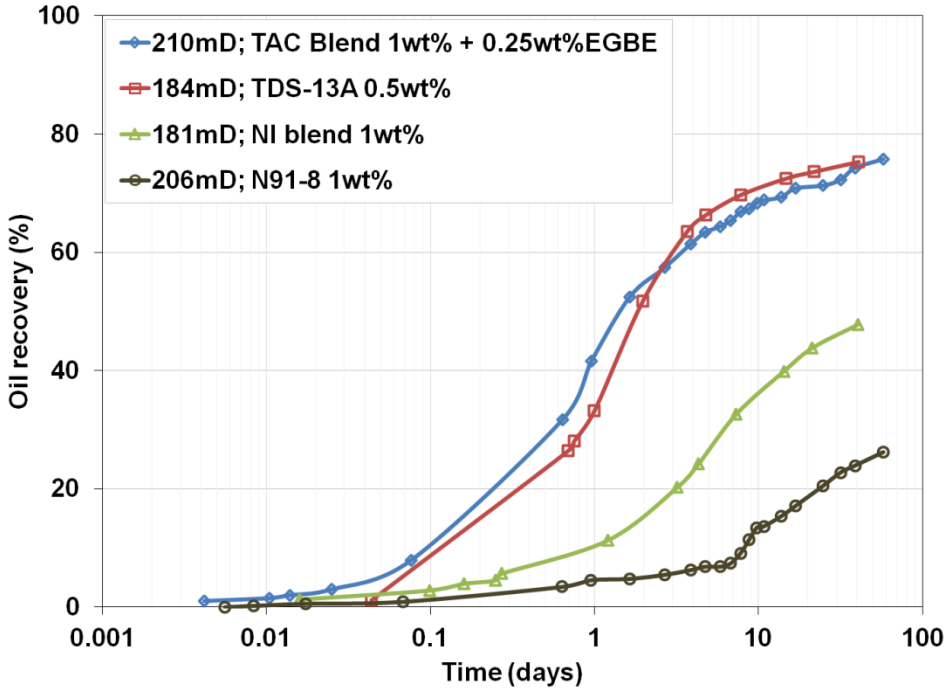

Figure 6 Imbibition history for various surfactant blends in dolomite outcrop cores at 25°C

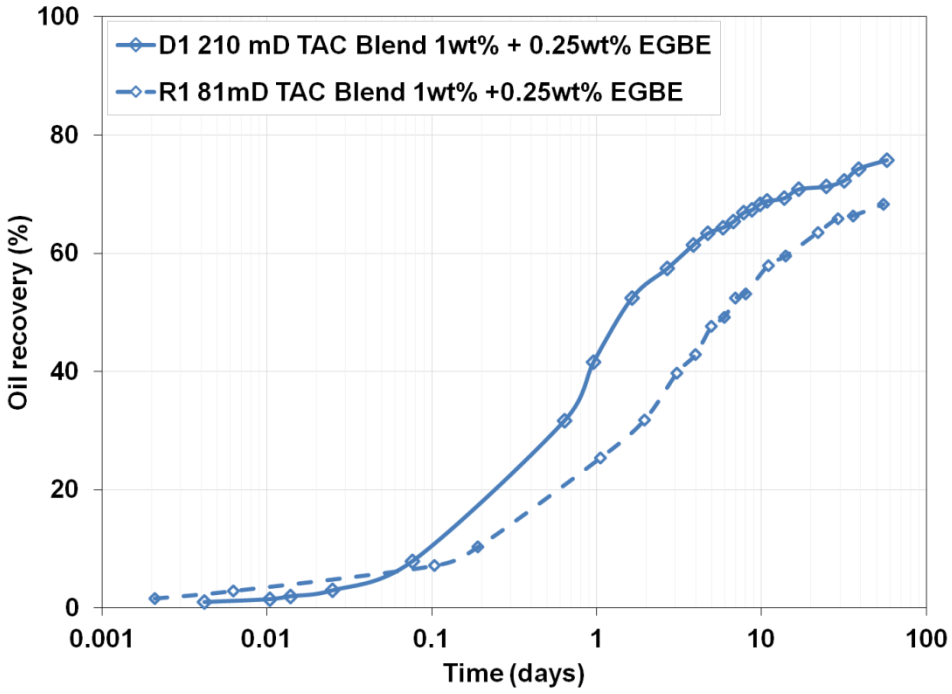

Figure 7 Imbibition history for TAC blend in dolomite outcrop and reservoir cores at 25°C.

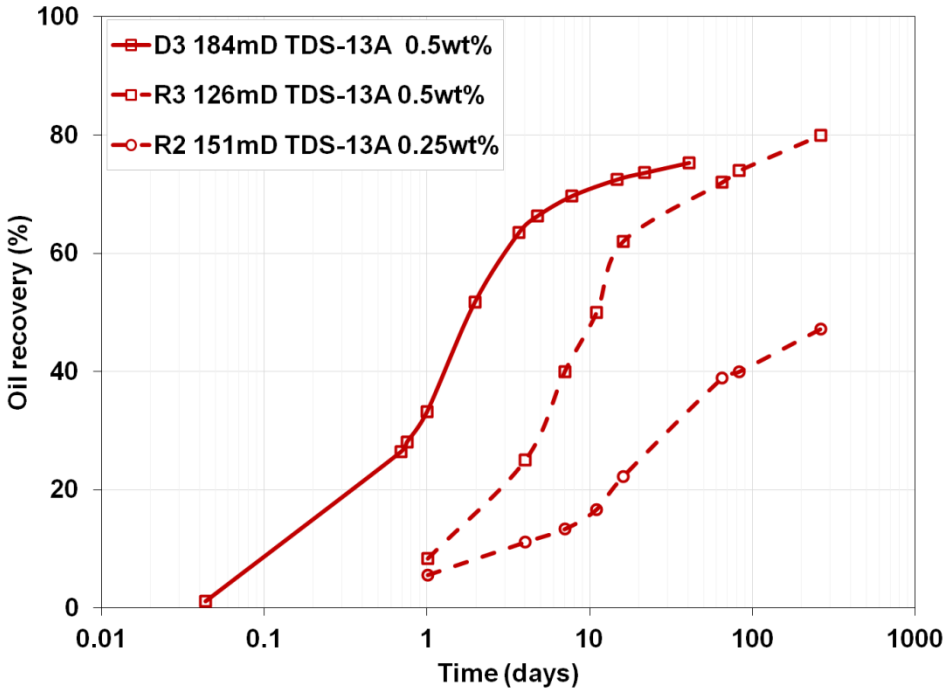

Figure 8 Imbibition history for TDS-13A in dolomite outcrop and reservoir cores, at different surfactant concentrations at 25°C.

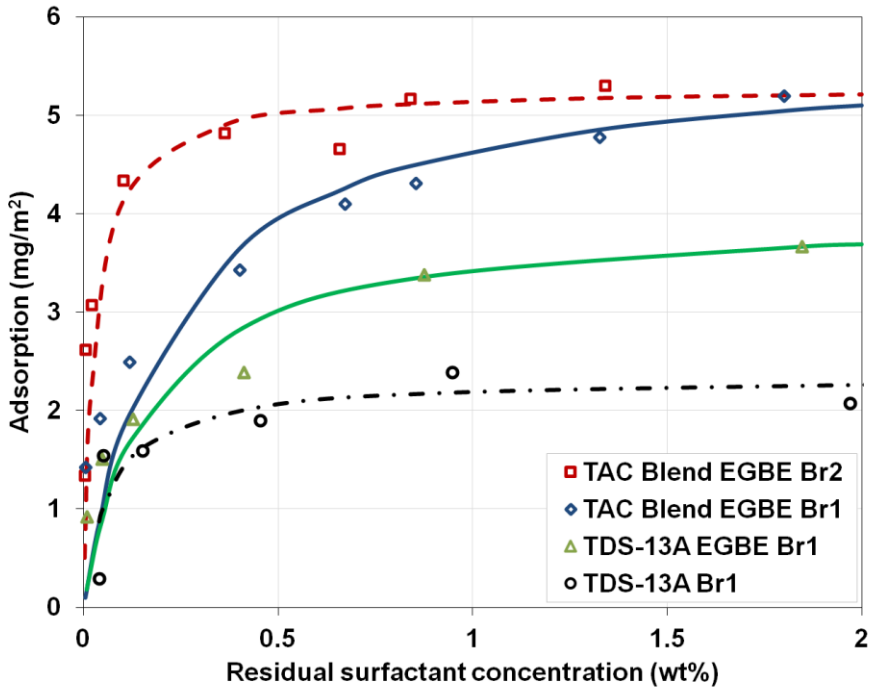

Figure 9 Static adsorption experiment for TDS-13A and TAC blend on dolomite powder at 25°C.

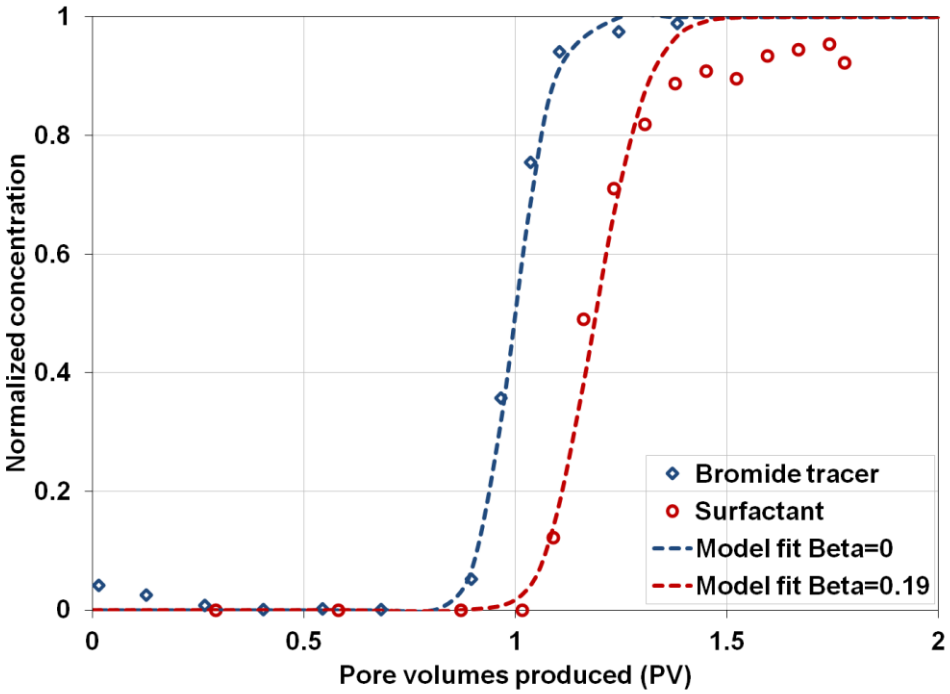

Figure 10 Dynamic adsorption experiment for TDS-13A in 102D limestone sandpack at 25°C.

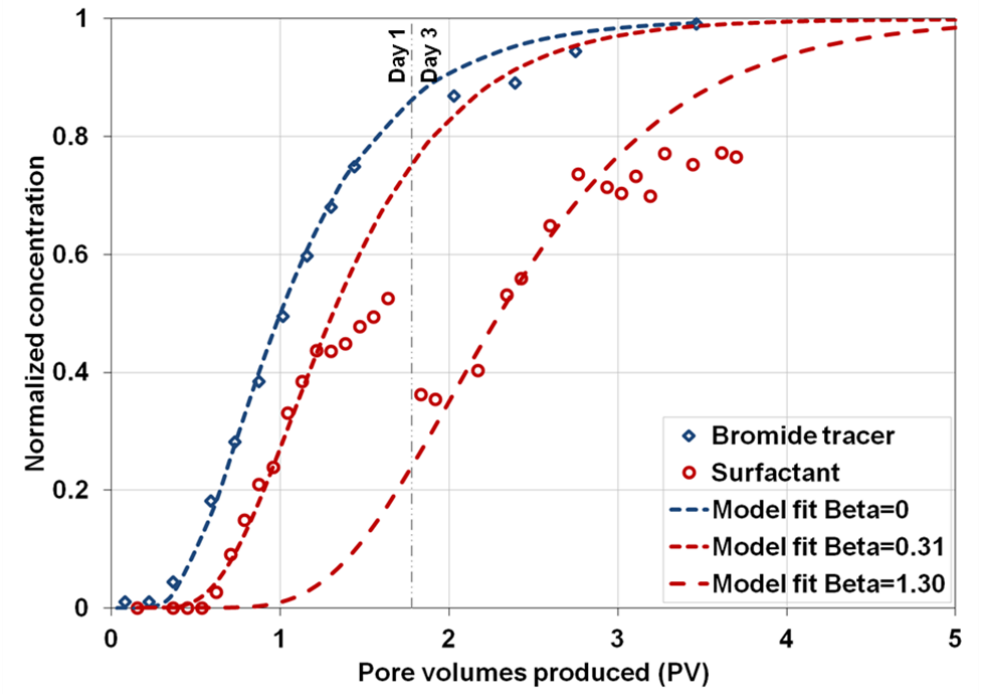

Figure 11 Dynamic adsorption experiment for TDS-13A in 6mD reservoir dolomite core at 25°C.

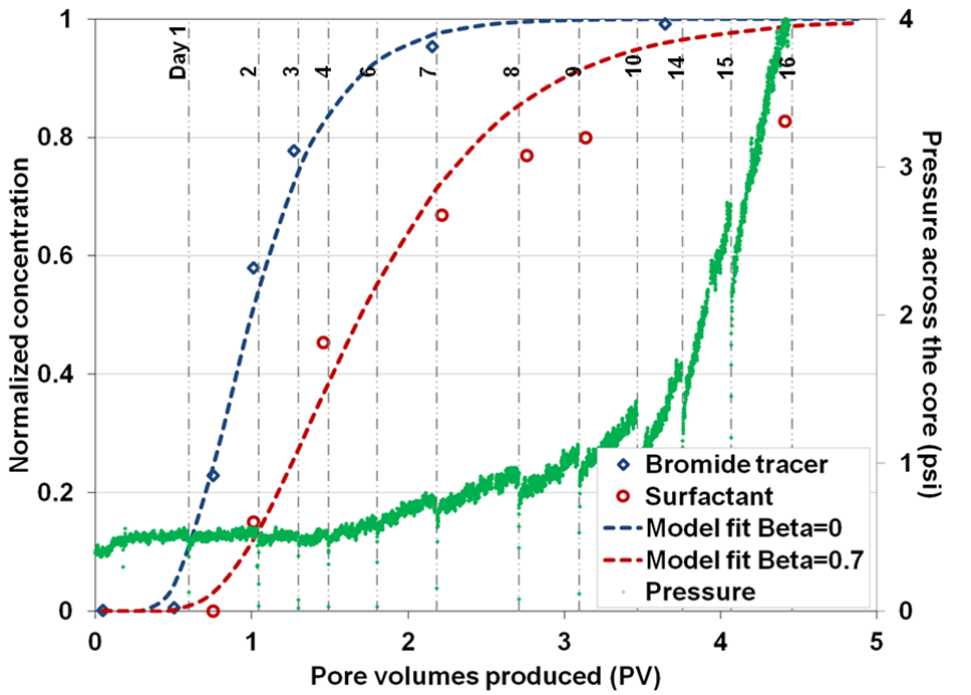

Figure 12 Dynamic adsorption experiment for TDS-13A in 15mD reservoir dolomite core at 25°C.

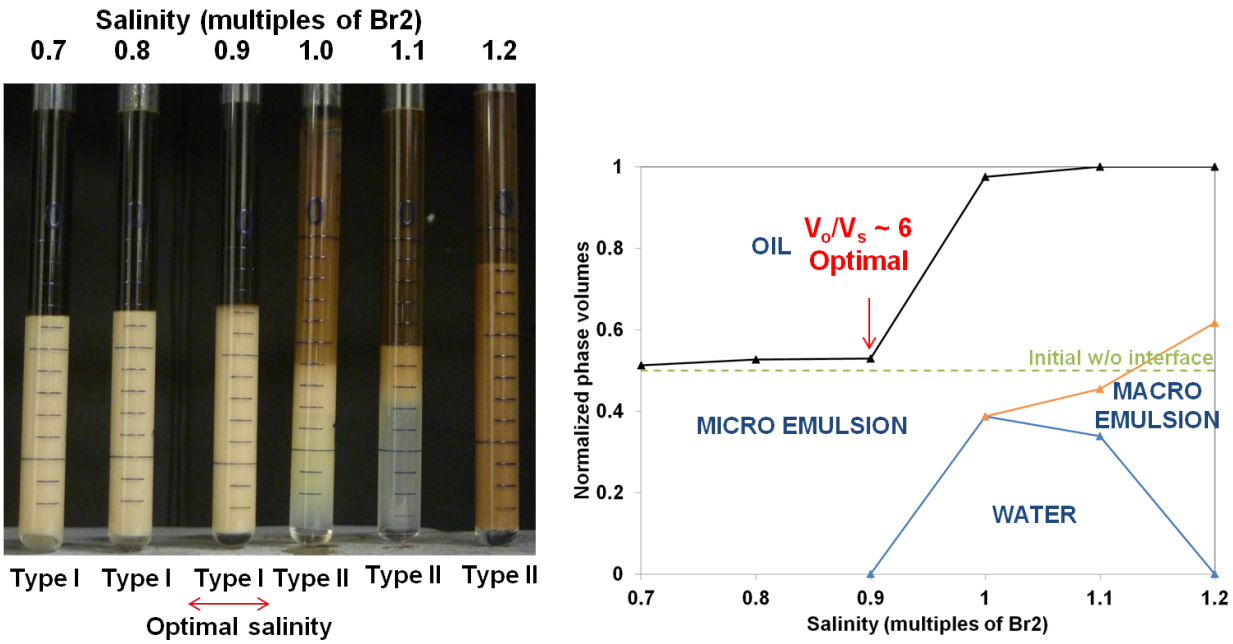

Figure 13 TDS-13A/S2 blend 1wt% with dead crude oil at 30°C

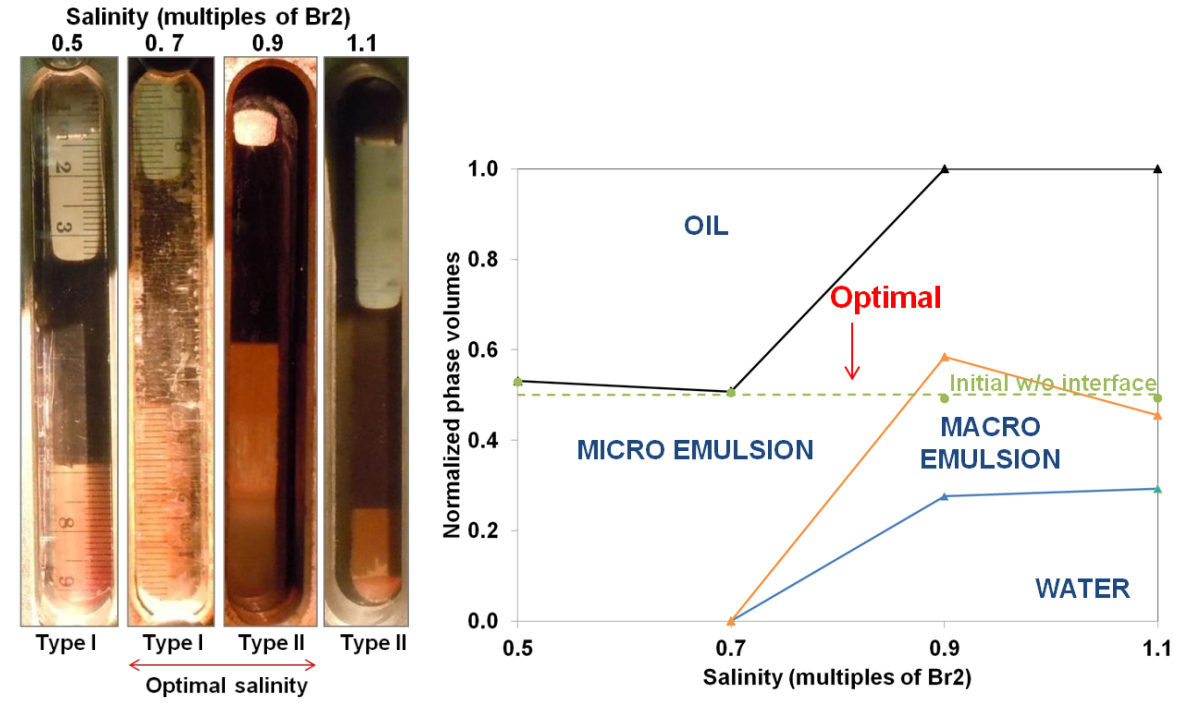

Figure 14 TDS-13A/S2 blend 1wt% with live crude oil at 30°C – 600psi methane

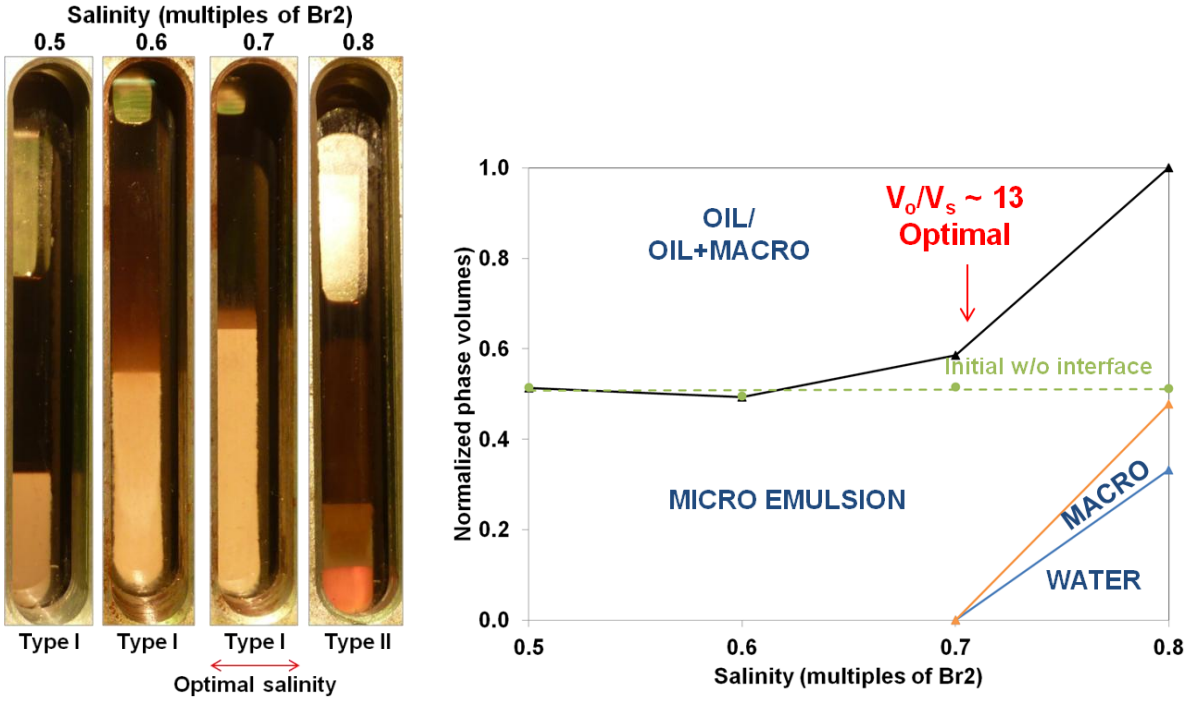

Figure 15 TDS-13A/S2 blend 1wt% with live crude oil at 30°C – 50psi ethane.

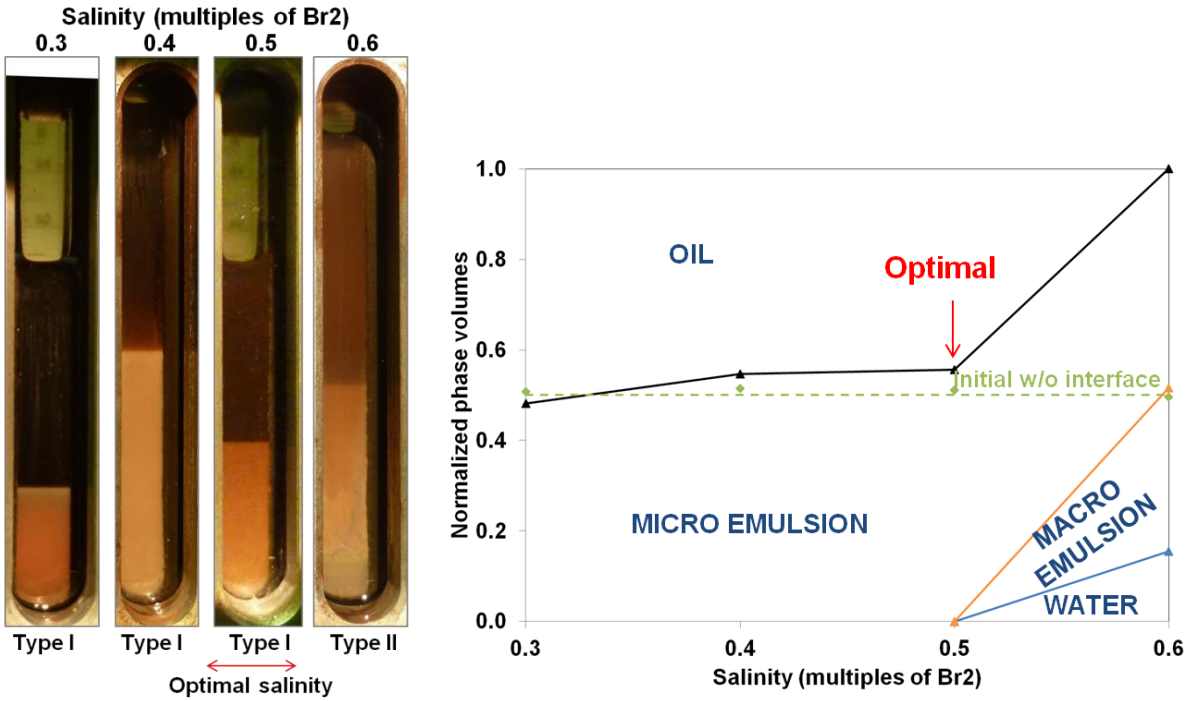

Figure 16 TDS-13A/S2 blend 1wt% with live crude oil at 30°C – 95psi ethane

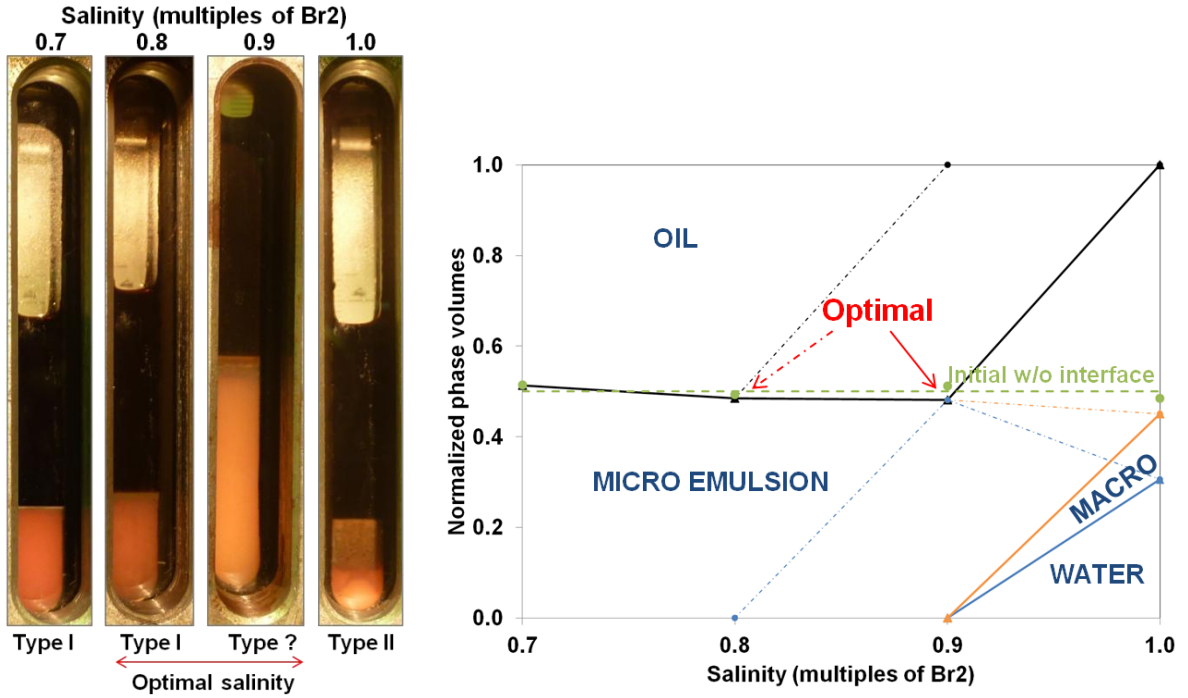

Figure 17 TDS-13A/S2 blend 1wt% with live crude oil at 30°C – 60psi carbon-dioxide. Phase map shows two alternate interpretations of the sample at 0.9Br2 and thus of optimal salinity.

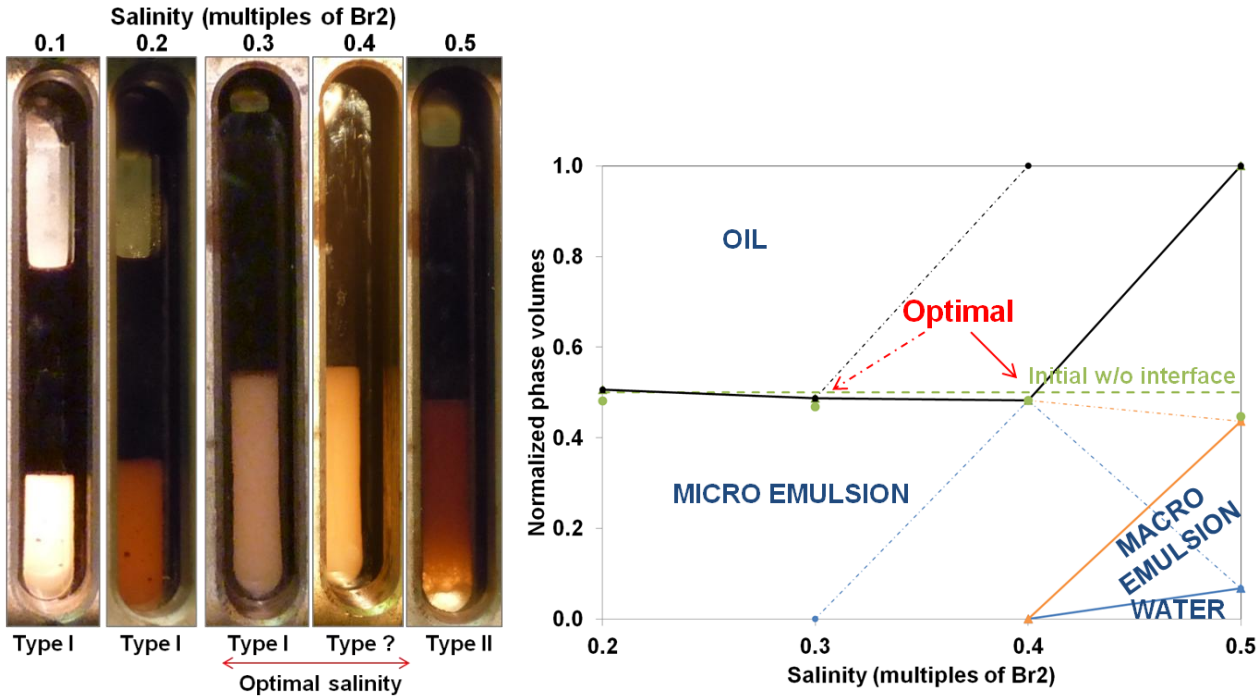

Figure 18 TDS-13A/S2 blend 1wt% with live crude oil at 30°C – 600psi carbon-dioxide. Phase map shows two alternate interpretations of the sample at 0.4Br2 and thus of optimal salinity.

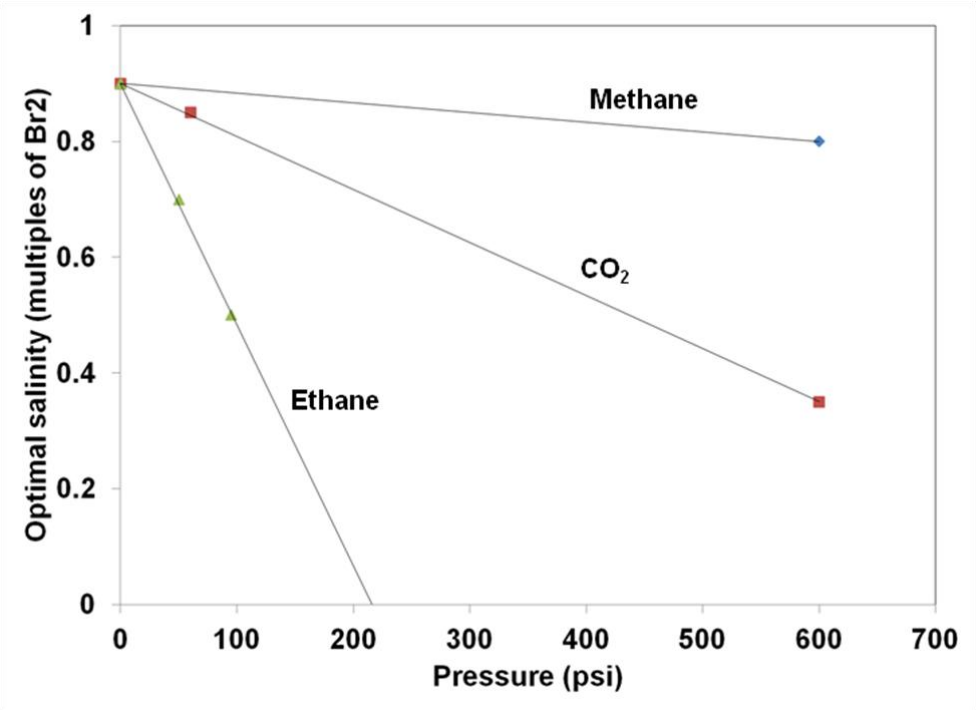

Figure 19 Optimal salinity of TDS-13A/S2 blend 1wt% as a function of pressure of solution gas at 30°C.

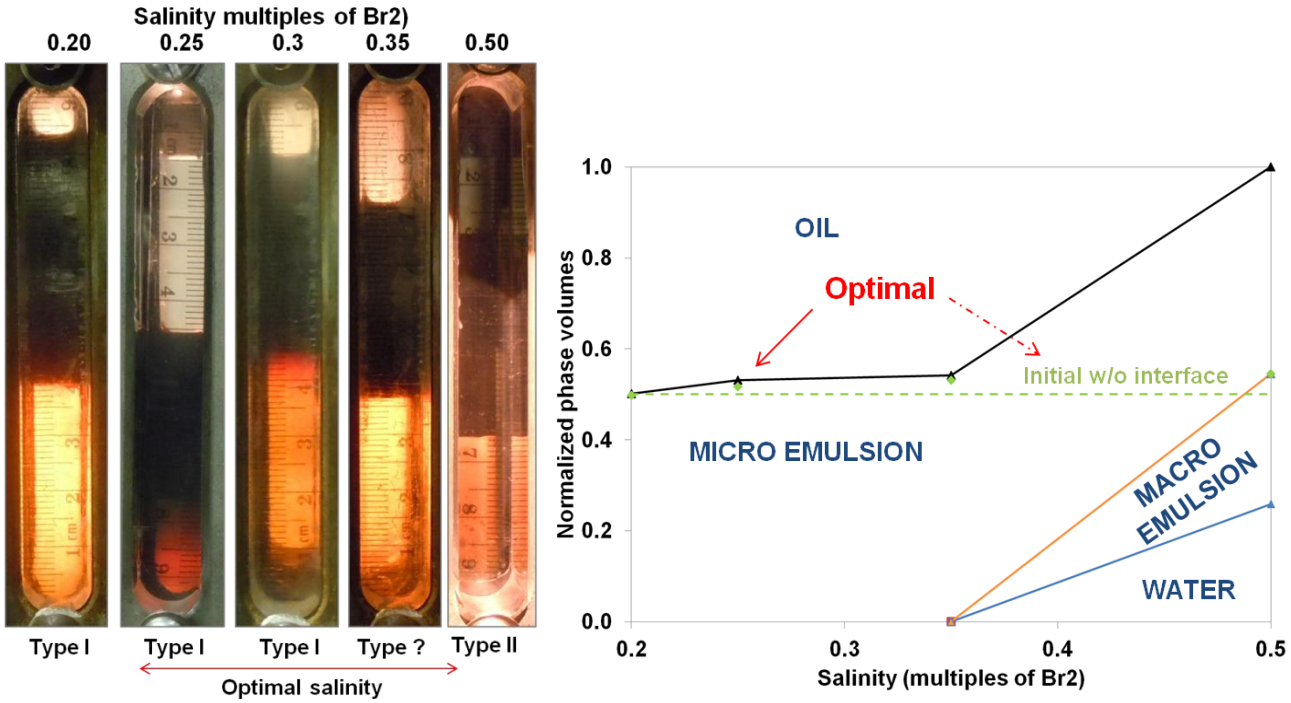

Figure 20 TDS-13A/S2 blend 1wt% with live crude oil at 30°C – 600psi separator gas. Phase map shows two alternate interpretations of the optimal salinity.